$B^*B\pi$ coupling using relativistic heavy quarks

J. M. Flynn,[1] P. Fritzsch,[2,*] T. Kawanai,[3,4,†] C. Lehner,[4] C. T. Sachrajda,[1] B. Samways,[1]
R. S. Van de Water,[5] and O. Witzel[6,‡]

(RBC and UKQCD Collaborations)

[1]*School of Physics and Astronomy, University of Southampton, Southampton SO17 1BJ, United Kingdom*
[2]*Institut für Physik, Humboldt Universität, 12489 Berlin, Germany*
[3]*RIKEN-BNL Research Center, Brookhaven National Laboratory, Upton, New York 11973, USA*
[4]*Physics Department, Brookhaven National Laboratory, Upton, New York 11973, USA*
[5]*Theoretical Physics Department, Fermi National Accelerator Laboratory, Batavia, Illinois 60510, USA*
[6]*Center for Computational Science, Boston University, Boston, Massachusetts 02215, USA*

We report on a calculation of the $B^*B\pi$ coupling in three-flavor lattice QCD. This coupling, defined from the strong-interaction matrix element $\langle B\pi|B^*\rangle$, is related to the leading order low-energy constant in heavy meson chiral perturbation theory. We carry out our calculation directly at the b-quark mass using a nonperturbatively tuned clover action that controls discretization effects of order $|\vec{p}a|$ and $(ma)^n$ for all n. Our analysis is performed on RBC/UKQCD gauge configurations using domain-wall fermions and the Iwasaki gauge action at two lattice spacings of $a^{-1} = 1.729(25)$ GeV, $a^{-1} = 2.281(28)$ GeV, and unitary pion masses down to 290 MeV. We achieve good statistical precision and control all systematic uncertainties, giving a final result for the coupling $g_b = 0.56(3)_{\text{stat}}(7)_{\text{sys}}$ in the continuum and at the physical light-quark masses. This is the first calculation performed directly at the physical b-quark mass and lies in the region one would expect from carrying out an interpolation between previous results at the charm mass and at the static point.

I. INTRODUCTION

The power of lattice QCD in probing the Standard Model and uncovering evidence for new physics lies predominantly in the flavor sector. To constrain the Cabibbo-Kobayashi-Maskawa (CKM) unitarity triangle [1–3] requires many inputs that must be evaluated nonperturbatively, particularly in the B-meson sector. For instance, an important constraint on the apex of the CKM unitarity triangle comes from neutral B-meson mixing, which gives information on the ratio of CKM elements $|V_{ts}|^2/|V_{td}|^2$. Accessing these CKM elements from the experimental data requires knowledge of the B-meson decay constant and bag parameter, or alternatively the SU(3) breaking ratio

$$\frac{f_{B_s}\sqrt{B_{B_s}}}{f_{B_d}\sqrt{B_{B_d}}}. \qquad (1)$$

Lattice calculations of the decay constants f_{B_d} and f_{B_s} are also necessary inputs for the Standard Model predictions of

BR$(B \to \tau\nu)$ and BR$(B_s \to \mu^+\mu^-)$ respectively, while lattice calculations of the $B \to \pi l\nu$ form factor allow a determination of the CKM matrix element $|V_{ub}|$. For both semileptonic form factors and mixing matrix elements, the precision of lattice calculations lags behind experiment. The experimental measurements will continue to improve with the large data sets available at Belle II and from LHCb. Therefore it is essential to reduce further the theoretical uncertainties in the nonperturbative hadronic parameters in order to maximize the scientific impact of current and future B-physics experiments.

A major source of uncertainty in all previous lattice calculations is from practical difficulties simulating at physical light-quark masses. Theoretical insight from heavy meson chiral perturbation theory (HMχPT) can guide extrapolations down to the physical point, but lack of knowledge of the low-energy constants (LECs) of the theory introduces uncertainties. For example, at next-to-leading order (NLO) in HMχPT and lowest order in the heavy-quark expansion the logarithmic dependence of f_{B_d} and B_{B_d} on the light-quark (or equivalently, pion) mass is given by [4,5]

$$f_{B_d} = F\left(1 - \frac{3}{4}\frac{1+3\hat{g}^2}{(4\pi f_\pi)^2}M_\pi^2 \log(M_\pi^2/\mu^2)\right) + \cdots, \quad (2)$$

$$B_{B_d} = B\left(1 - \frac{1}{2}\frac{1-3\hat{g}^2}{(4\pi f_\pi)^2}M_\pi^2 \log(M_\pi^2/\mu^2)\right) + \cdots, \quad (3)$$

*Present address: Instituto de Física Teórica UAM/CSIC, Universidad Autónoma de Madrid, E-28049 Madrid, Spain.
†Present address: Forschungszentrum Jülich, Institute for Advanced Simulation, Jülich Supercomputing Centre, 52425 Jülich, Germany.
‡Present address: Higgs Centre for Theoretical Physics, School of Physics & Astronomy, The University of Edinburgh, Edinburgh EH9 3FD, United Kingdom.

014510-1

where $\hat{g}$ is the leading-order LEC. The strong-interaction matrix element $\langle B\pi|B^*\rangle$ is used to determine a coupling g_b, which would become $\hat{g}$ in the static limit of an infinitely heavy b quark. At the order used above in Eqs. (2) and (3), we are free to use g_b in place of $\hat{g}$; differences between the two are of order $1/m_b$.

In this paper we perform the first calculation of the coupling g_b directly at the b-quark mass. Previous determinations of the coupling have been hindered by the difficulties of simulating heavy quarks on the lattice. Lattice calculations have been performed for g_c, the analogous coupling for D-mesons [6–9], and for $\hat{g}$ itself [7,10–13]. Having a reliable theoretical calculation of the coupling for the B system is important since this coupling cannot be accessed directly through experiment. The strong coupling $g_{D^*D\pi}$ has been measured by the CLEO collaboration [14,15] and more recently by *BABAR* [16,17], but with B-mesons there is not enough phase space for the $B^* \to B\pi$ decay to occur. Model estimates exist for g_b, including from QCD sum rules [18–21] and nonrelativistic quark models [22].

The rest of this paper is organized as follows. In Sec. II we briefly review the framework of HMχPT, show how g_b enters and present the method for extracting g_b from lattice matrix-element calculations. Section III describes the parameters of the light-quark, gluon, and heavy-quark actions used in the numerical calculation and presents the ratios of two- and three-point correlators used to obtain g_b. In Sec. IV we fit the correlator ratios to extract g_b and then extrapolate these results to the continuum and physical quark masses using SU(2) HMχPT. We estimate the systematic errors in g_b in Sec. V, discussing each source of uncertainty in a different subsection. We conclude in Sec. VI by presenting our final results and error budget, and comparing our result to other similar calculations.

II. HEAVY MESON CHIRAL PERTURBATION THEORY

In the infinite heavy-quark mass limit the properties of heavy-light mesons become independent of the heavy quark's spin and flavor quantum numbers. Combining this with the chiral symmetry present in the massless light-quark ($m_q \to 0$) limit of QCD provides the basis for heavy meson chiral perturbation theory. This effective theory of QCD is a joint expansion in powers of the inverse heavy-quark mass $1/m_Q$ and the light-quark-mass m_q.

In HMχPT the heavy-light pseudoscalar and vector mesons, P and P^*, are combined in a covariant 4×4 matrix representation,

$$H = \frac{1+\mathcal{v}}{2}(P_\mu^*\gamma^\mu - P\gamma_5). \qquad (4)$$

If one includes three light dynamical quark flavors (u, d, s), this corresponds to SU(3) HMχPT with the usual octet

of pseudo-Nambu-Goldstone bosons for the light pseudoscalars:

$$\mathcal{M} = \begin{pmatrix} \frac{1}{\sqrt{2}}\pi^0 + \frac{1}{\sqrt{6}}\eta & \pi^+ & K^+ \\ \pi^- & -\frac{1}{\sqrt{2}}\pi^0 + \frac{1}{\sqrt{6}}\eta & K^0 \\ K^- & \bar{K}^0 & -\sqrt{\frac{2}{3}}\eta \end{pmatrix}. \qquad (5)$$

Because the strange-quark mass is almost 30 times larger than the average up-down quark mass, however, one can also treat the strange quark as heavy and include only the up- and down-quark dynamical degrees of freedom; this leads to SU(2) HMχPT (with the corresponding modification of $\mathcal{M}$). At lowest order the interactions between the heavy and light mesons are determined by a Lagrangian with a single LEC [23,24],

$$\mathcal{L}_{\text{HM}\chi\text{PT}}^{\text{int}} = \hat{g}\text{Tr}(\bar{H}_a H_b \mathcal{A}_{ba}^\mu \gamma_\mu \gamma_5), \qquad (6)$$

where

$$\mathcal{A}_\mu = \frac{i}{2}(\xi^\dagger \partial_\mu \xi - \xi \partial_\mu \xi^\dagger) \qquad (7)$$

and $\xi = \exp(i\mathcal{M}/f_\pi)$. The roman indices run over light-quark flavor and the trace is over Dirac indices. We use a convention where $f_\pi \approx 130$ MeV.

The matrix element for the strong transition $B^* \to B\pi$ is parametrized by $g_{B^*B\pi}$,

$$\langle B(p')\pi(q)|B^*(p,\lambda)\rangle = g_{B^*B\pi}q \cdot \epsilon^{(\lambda)}(p), \qquad (8)$$

where $q = p - p'$ and $\epsilon^{(\lambda)}(p)$ is the polarization vector for polarization state labeled by λ. Evaluating the same matrix element at leading order in HMχPT,

$$\langle P(p')\pi(q)|P^*(p,\lambda)\rangle = \frac{2M_P}{f_\pi}\hat{g}q \cdot \epsilon^{(\lambda)}(p), \qquad (9)$$

enables the determination of g_b from

$$g_{B^*B\pi} = \frac{2M_B}{f_\pi}g_b, \qquad (10)$$

with g_b equal to $\hat{g}$ up to $1/m_b^n$ corrections.

Performing a Lehmann-Symanzik-Zimmermann reduction and using the partially conserved axial current relation for a soft pion, Eq. (8) becomes

$$g_{B^*B\pi}q \cdot \epsilon^{(\lambda)}(p)$$
$$= iq_\mu \frac{M_\pi^2 - q^2}{f_\pi M_\pi^2} \int d^4x e^{iq\cdot x}\langle B(p')|A^\mu(x)|B^*(p,\lambda)\rangle,$$

$$(11)$$

where $A^\mu = \bar{\psi}_1 \gamma^\mu \gamma_5 \psi_2$ is the light-quark axial-vector current. Using a form-factor decomposition of the matrix element

$$\langle B(p')|A^\mu|B^*(p,\lambda)\rangle$$

$$= 2M_{B^*} A_0(q^2) \frac{\epsilon^{(\lambda)} \cdot q}{q^2} q^\mu$$

$$+ (M_{B^*} + M_B) A_1(q^2) \left[\epsilon^{(\lambda)\mu} - \frac{\epsilon^{(\lambda)} \cdot q}{q^2} q^\mu \right]$$

$$+ A_2(q^2) \frac{\epsilon^{(\lambda)} \cdot q}{M_{B^*} + M_B} \left[p^\mu + p'^\mu - \frac{M_{B^*}^2 - M_B^2}{q^2} q^\mu \right], \quad (12)$$

we see that at $q^2 = 0$,

$$g_{B^*B\pi} = \frac{2M_{B^*} A_0(0)}{f_\pi}. \quad (13)$$

On the lattice, we cannot simulate exactly at $q^2 = 0$ without using twisted boundary conditions. Furthermore and from Eq. (11), we see that the form factor A_0 contains a pole at the pion mass, so it will be difficult to do a controlled extrapolation to $q^2 = 0$. However, the decomposition in Eq. (12) must be free of unphysical poles, which allows us to obtain the relation

$$g_{B^*B\pi} = \frac{1}{f_\pi} [(M_{B^*} + M_B) A_1(0) + (M_{B^*} - M_B) A_2(0)]. \quad (14)$$

The A_1 term is expected to dominate because the relative contribution of A_2 is suppressed by the ratio $(M_{B^*} - M_B)/(M_{B^*} + M_B)$ whose value is 0.004 for the physical B and B^* masses. It is this relation that we use for our numerical calculation.

III. CALCULATIONAL STRATEGY

A. Light quarks and gauge fields

Our analysis is carried out using ensembles produced by the RBC and UKQCD collaborations [25,26] with the Iwasaki gauge action [27,28] and $2 + 1$ flavor dynamical domain-wall fermions [29,30]. The configurations are at two lattice spacings, the finer 32^2 ensembles have an inverse lattice spacing of $a^{-1} = 2.281(28)$ GeV and the coarser 24^3 ensembles have $a^{-1} = 1.729(25)$ GeV, corresponding to approximately 0.086 and 0.11 fm respectively. All ensembles have a spatial extent of 2.6 fm. We simulate with unitary light quarks corresponding to pion masses down to $M_\pi = 289$ MeV. On all ensembles the strange sea-quark mass is tuned to within 10% of its physical value. The fifth dimensional extent of both lattices is $L_S = 16$, corresponding to a residual quark mass of $m_{res}a = 0.003152$ on the 24^3 ensembles and $m_{res}a = 0.0006664$ on the 32^3 ensembles. The lattice quark masses corresponding to the physical u/d and s quarks are $\tilde{m}_{u/d}a = 0.00136(4)$, $\tilde{m}_s a = 0.0379(11)$

TABLE I. Lattice simulation parameters. All ensembles are generated using $2 + 1$ flavors of domain-wall fermions and the Iwasaki gauge action. All valence pion masses are equal to the sea-pion mass.

L/a	a/fm	$m_l a$	$m_s a$	# configs	# sources	M_π/MeV
24	0.11	0.005	0.04	1636	1	329
24	0.11	0.010	0.04	1419	1	419
24	0.11	0.020	0.04	345	1	558
32	0.08	0.004	0.03	628	2	289
32	0.08	0.006	0.03	889	2	345
32	0.08	0.008	0.03	544	2	394

on the 24^3 ensembles and $\tilde{m}_{u/d}a = 0.00102(5)$, $\tilde{m}_s a = 0.0280(7)$ on the 32^3 ensembles. The tildes indicate that these values include the residual quark mass.

Our calculation makes use of unitary light-quark propagators with point sources previously generated as part of the RBC/UKQCD B-physics program [31–35]. Full details of the ensembles and propagators used are presented in Table I. We perform a random translation on each gauge field configuration to minimize the effects of autocorrelations on our results, allowing us to use more closely spaced trajectories and gain statistics. For each configuration in the 32^3 ensembles we use propagators computed at two time sources separated by half the lattice temporal extent to compensate for the smaller ensemble sizes.

B. Bottom quarks

Simulating heavy quarks on the lattice presents the problem of dealing with $m_Q a \geq 1$. A number of approaches have been developed to tackle this problem. In the limit of infinite mass the quarks become a static source of color charge and their lattice propagator reduces to a trace of a product of temporal gauge links. This is the static action of Eichten and Hill [36] which has been used extensively to calculate the coupling g_∞, most recently in [13,37]. Another approach is nonrelativistic QCD [38], where the usual QCD Lagrangian is expanded in powers of v/c.

Here we use the relativistic heavy-quark (RHQ) action [39–41] to simulate fully relativistic bottom quarks while controlling discretization effects. Although $m_Q a$ is large for the heavy quark in a heavy-light meson, the spatial momentum $|\vec{p}a|$ is of $O(a\Lambda_{QCD})$. The RHQ action is an anisotropic Wilson action with a Sheikholeslami-Wohlert term [42]

$$S_{RHQ} = a^4 \sum_{x,y} \bar{\psi}(y) \left(m_0 + \gamma_0 D_0 + \zeta \vec{\gamma} \cdot \vec{D} - \frac{a}{2}(D_0)^2 \right.$$

$$\left. - \frac{a}{2}\zeta(\vec{D})^2 + \sum_{\mu\nu} \frac{ia}{4} c_p \sigma_{\mu\nu} F_{\mu\nu} \right)_{y,x} \psi(x). \quad (15)$$

El-Khadra, Kronfeld and Mackenzie showed that, for correctly tuned parameters, the anisotropic Clover action can be

TABLE II.   Tuned RHQ parameters for *b* quarks from Ref. [31]. The uncertainties shown are statistical, heavy-quark discretization effects, lattice-scale uncertainty, and from experimental inputs (the spin-averaged B_s-meson mass and B_s hyperfine splitting) respectively.

a/fm	$m_0 a$	c_p	ζ
0.11	8.45(6)(13)(50)(7)	5.8(1)(4)(4)(2)	3.10(7)(11)(9)(0)
0.08	3.99(3)(6)(18)(3)	3.57(7)(22)(19)(14)	1.93(4)(7)(3)(0)

used to describe heavy quarks with controlled cutoff effects to all orders in $m_Q a$ and of $O(|\vec{p}a|)$ [39]. Christ, Li, and Lin [41] later showed that only three independent parameters need to be determined and, further, presented a
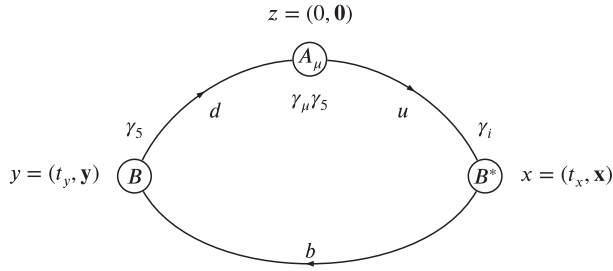

FIG. 1.   Quark flow diagram.

method for performing this parameter tuning nonperturbatively [43].

This tuning has been completed for *b* quarks [31] on the RBC/UKQCD configurations and those results (Table II) are exploited in this calculation. The heavy-quark propagators and the correlation functions used in this analysis are calculated using the CHROMA software library [44]. We apply Gaussian smearing to the heavy-quark propagators using parameters tuned in [31]. Because the correlators become very small at large time separations owing to the large masses in the exponentials, we run the inverter for the heavy quark propagators to a very small relative residual (10^{-45}). We found that pursuing the conjugate gradient iteration to this small residual is equivalent to demanding convergence separately for the residual on each time slice.

C. Three-point correlation functions

The matrix element that we wish to calculate in Eq. (12) corresponds to the quark-flow diagram shown in Fig. 1. To fully benefit from the available precalculated light-quark propagators, we arrange the calculation so that the axial-vector current is positioned at the light-quark propagator's source. This means that we use the
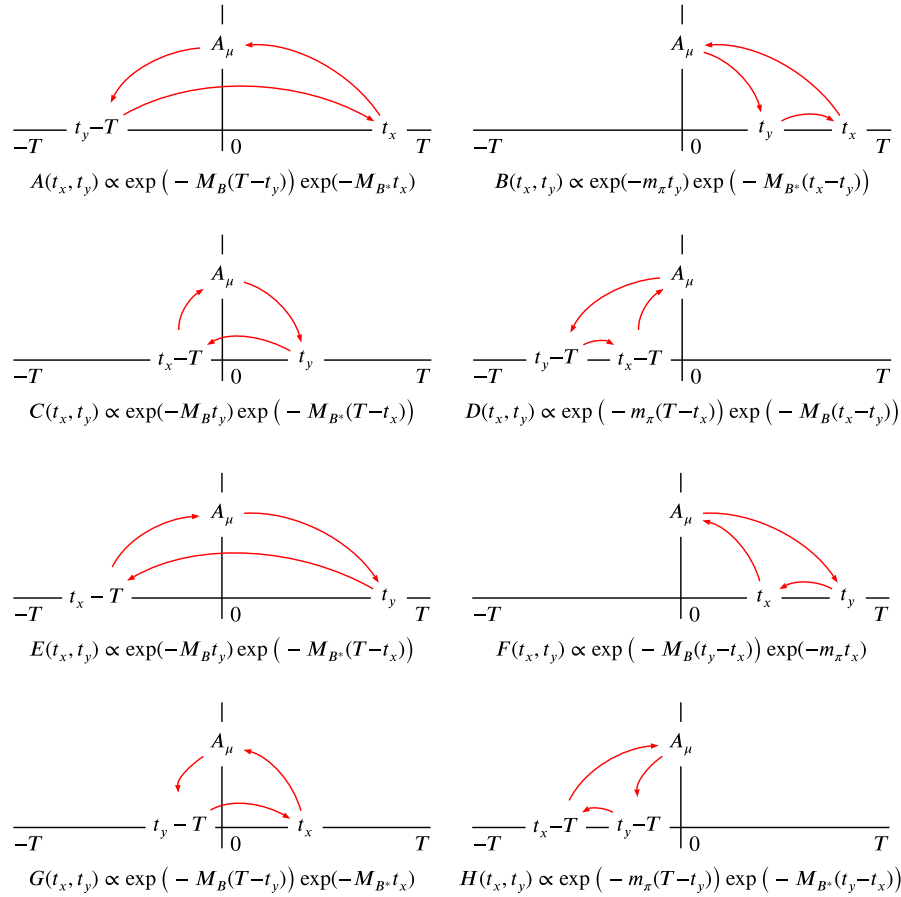

FIG. 2.   Leading contributions to the three-point correlator for $t_x > t_y$ (A, B, C, D) and $t_x \leq t_y$ (E, F, G, H).
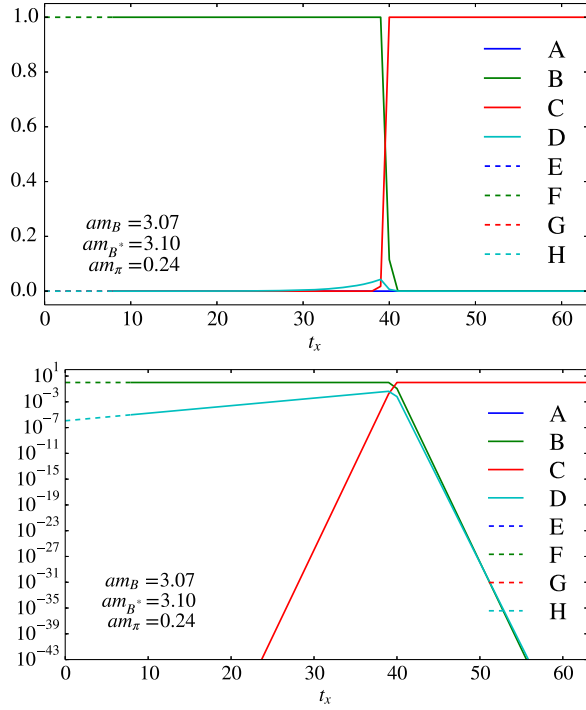
FIG. 3. The estimated relative sizes, with $t_y = 8$, of the eight contributions to the $B^*B\pi$ three-point function arising from different Wick contractions, using a linear scale (top) and log scale (bottom). Each contribution is scaled by dividing by the maximum contribution at that time. The matrix element of interest comes from C which is shown as a solid red line on both plots. This contribution dominates for large t_x.

$$C^{(3)}_{\mu\nu}(t_x, t_y; \vec{p}, \vec{p}\,')$$
$$= \sum_{\vec{x}, \vec{y}} e^{-i\vec{p}\cdot\vec{x} - i\vec{p}\,'\cdot\vec{y}} \text{Tr}[S_l(0,y)\gamma_5 S_h(y,x)\gamma_\nu S_l(x,0)\gamma_\mu\gamma_5]. \quad (16)$$

Because of the periodicity of the lattice there are further possible contributions beyond the desired Wick contraction in Fig. 1. An operator located at time t can also be considered at location $t - T$, where T is the lattice's temporal extent. If we take into account separately the cases where $t_x > t_y$ and $t_x \leq t_y$, there are eight possible contributing arrangements (considering $t + nT$ for integer n gives further contributions, but for increasing $|n|$ these are more and more suppressed). These are shown in Fig. 2. Using the approximation that the ground states immediately dominate the time dependence and that the matrix elements are all unity, we can estimate the time dependence of the three-point correlation function:

$$C^{(3)}(t_x, t_y)$$
$$= \begin{cases} A(t_x, t_y) + B(t_x, t_y) + C(t_x, t_y) + D(t_x, t_y) & t_x > t_y, \\ E(t_x, t_y) + F(t_x, t_y) + G(t_x, t_y) + H(t_x, t_y) & t_x \leq t_y. \end{cases}$$
$$(17)$$

It is expected that the signal from which to extract the $B^*B\pi$ coupling will be seen at large t_x (approaching T from below), coming from the contribution shown as $C(t_x, t_y)$ in Fig. 2. Figure 3 shows the relative size of the different contributions as a function of t_x with all matrix elements set to unity. As anticipated, C is the dominant contribution in a region $T/2 + t_y < t_x < T$. This result appears steady for a range of the masses M_B, M_{B^*}, M_π. Plotting the sum of the contributions as a function of t_x (setting all matrix elements to unity) we see a peak at $t_x = t_y$ and an overall cosh-like form shifted by t_y as shown on the right in Fig. 4. On the left of Fig. 4 we show good agreement with this form for our numerical data, with t_y the time position of the source for the sequential inversion. This gives us confidence that we can

periodicity of the lattice, creating the B^* meson at large time t_x, propagating to the origin at $t = 0$, where the current acts and continuing to small time t_y, where the B-meson is annihilated. With this setup, we need only one inversion, a heavy-quark propagator calculated from t_y, using a light-quark propagator for the sequential source. The necessary trace is
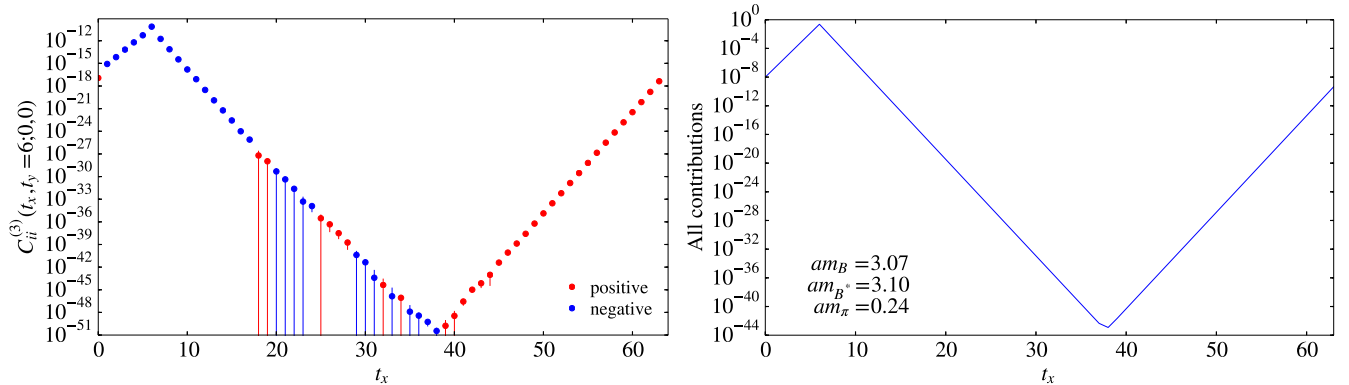

FIG. 4. The three-point correlator of Eq. (18) evaluated on the 24^3, $m_l a = 0.005$ ensemble with $t_y = 6$ (left). The time dependence closely matches that predicted from the analysis in Sec. III C (right).

extract the desired matrix element from the large t_x region of the three-point correlator.

D. Ratios

To access the matrix element in Eq. (12) we calculate the lattice three-point function,

$$
\begin{aligned}
C^{(3)}_{\mu\nu}(t_x, t_y; \vec{p}, \vec{p}') &= \sum_{\vec{x},\vec{y}} e^{-i\vec{p}\cdot\vec{x}} e^{-i\vec{p}'\cdot\vec{y}} \langle B(y) A_\nu(0) B^*_\mu(x) \rangle \\
&\overset{\substack{T-t_x>0 \\ t_y>0}}{\approx} \sum_\lambda \frac{Z_B^{1/2} Z_{B^*}^{1/2}}{2E_B 2E_{B^*}} \langle B(p')|A_\nu|B^*(p,\lambda)\rangle \\
&\quad \times \epsilon^{(\lambda)}_\mu e^{-E_B t_y - E_{B^*}(T-t_x)},
\end{aligned}
\tag{18}
$$

and the vector and pseudoscalar two-point functions,

$$
C^{(2)}_{BB}(t; \vec{p}) = \sum_{\vec{x}} e^{-i\vec{p}\cdot\vec{x}} \langle B(x)B(0)\rangle \approx Z_B \frac{e^{-E_B t}}{2E_B}, \tag{19}
$$

$$
\begin{aligned}
C^{(2)}_{B^*_\mu B^*_\nu}(t; \vec{p}) &= \sum_{\vec{x}} e^{-i\vec{p}\cdot\vec{x}} \langle B^*_\nu(x) B^*_\mu(0)\rangle \\
&\approx Z_{B^*} \frac{e^{-E_{B^*} t}}{2E_{B^*}} \left(\delta_{\mu\nu} - \frac{p_\mu p_\nu}{p^2}, \right).
\end{aligned}
\tag{20}
$$

If we set both the vector and pseudoscalar momenta to zero in Eq. (18), such that $\vec{q} = \vec{p} = \vec{p}' = 0$ and $q^2 = q_0^2 = (M_{B^*} - M_B)^2 \approx 0$, we can see from Eq. (12) that the only form factor accessible is A_1. Hence we form the ratio (not summed on i):

$$
\begin{aligned}
R_1(t_x, t_y) &= \frac{C^{(3)}_{ii}(t_x, t_y; \vec{p}=0, \vec{p}'=0) Z_B^{1/2} Z_{B^*}^{1/2}}{C^{(2)}_{BB}(t_y; \vec{p}=0) C^{(2)}_{B^*_i B^*_i}(T-t_x; \vec{p}=0)} \\
&= (M_{B^*} + M_B) A_1(q_0^2),
\end{aligned}
\tag{21}
$$

where we can average over the three spatial directions ($i = 1, 2, 3$). To access the other form factors we need to inject a unit of momentum, such that $\vec{q} = \vec{p} = (1, 0, 0) \times 2\pi/L$ and $\vec{p}' = 0$. Following [6], we define the ratios:

$$
\begin{aligned}
R_2(t_x, t_y) &= \frac{C^{(3)}_{10}(t_x, t_y; \vec{p}\neq 0, \vec{p}'=0) Z_B^{1/2} Z_{B^*}^{1/2}}{C^{(2)}_{BB}(t_y; \vec{p}'=0) C^{(2)}_{B^*_2 B^*_2}(T-t_x; \vec{p}\neq 0)} \\
&= \sum_\lambda \langle B(p')|A_0|B^*(p,\lambda)\rangle \epsilon^{(\lambda)}_1,
\end{aligned}
\tag{22}
$$

$$
\begin{aligned}
R_3(t_x, t_y) &= \frac{C^{(3)}_{11}(t_x, t_y; \vec{p}\neq 0, \vec{p}'=0) Z_B^{1/2} Z_{B^*}^{1/2}}{C^{(2)}_{BB}(t_y; \vec{p}'=0) C^{(2)}_{B^*_2 B^*_2}(T-t_x; \vec{p}\neq 0)} \\
&= \sum_\lambda \langle B(p')|A_1|B^*(p,\lambda)\rangle \epsilon^{(\lambda)}_1,
\end{aligned}
\tag{23}
$$

$$
\begin{aligned}
R_4(t_x, t_y) &= \frac{C^{(3)}_{22}(t_x, t_y; \vec{p}\neq 0, \vec{p}'=0) Z_B^{1/2} Z_{B^*}^{1/2}}{C^{(2)}_{BB}(t_y; \vec{p}'=0) C^{(2)}_{B^*_2 B^*_2}(T-t_x; \vec{p}\neq 0)} \\
&= \sum_\lambda \langle B(p')|A_2|B^*(p,\lambda)\rangle \epsilon^{(\lambda)}_2 \\
&= (M_{B^*} + M_B) A_1(q^2).
\end{aligned}
\tag{24}
$$

These allow access to the form factor A_2 through

$$
\begin{aligned}
\frac{A_2}{A_1} &= \frac{(M_{B^*} + M_B)^2}{2M_B^2 q_1^2} \left[-q_1^2 + E_{B^*}(E_{B^*} - M_B) \right. \\
&\quad \left. - \frac{M_{B^*}^2 (E_{B^*} - M_B)}{E_{B^*}} \frac{R_3}{R_4} - i \frac{M_{B^*}^2 q_1}{E_{B^*}} \frac{R_2}{R_4} \right].
\end{aligned}
\tag{25}
$$

The ratio in Eq. (25) is obtained at nonzero values of q^2 and needs to be extrapolated to $q^2 = 0$. However, from Eq. (14) the contribution of $A_2(0)$ relative to $A_1(0)$ is suppressed by the ratio $(M_{B^*} - M_B)/(M_{B^*} + M_B)$. The form factor A_1 is obtained at $q_0^2 = (M_{B^*} - M_B)^2$ from Eq. (21), but examination shows that the slight extrapolation to $q^2 = 0$ is not necessary at the resolution possible with the available statistics. If we define functions G_1 and G_2,

$$
\begin{aligned}
G_1(q^2) &= (M_{B^*} + M_B) A_1(q^2), \\
G_2(q^2) &= (M_{B^*} - M_B) A_2(q^2),
\end{aligned}
\tag{26}
$$

we can write the coupling as $G_1(0)$ plus a small correction from the ratio G_2/G_1,

$$
g_b = \frac{Z_A}{2M_B} G_1(0) \left(1 + \frac{G_2(0)}{G_1(0)}\right), \tag{27}
$$

where Z_A is the light axial-vector current renormalization factor. In our simulations A_2 is of comparable size to A_1. The mass suppression in the ratio G_2/G_1 means that the correction term in (27) is at most 2% on our ensembles and typically at the subpercent level, with an error comparable to its size.

We take Z_A from the RBC/UKQCD combined analysis of the light hadron spectrum, pseudoscalar meson decay constants and quark masses on the 24^3 and 32^3 ensembles [26]. The values are calculated from the ratio of the conserved and local vector currents, extrapolated to the chiral limit and are shown in Table III.

TABLE III. Axial current renormalization factors used in this work, calculated in [26].

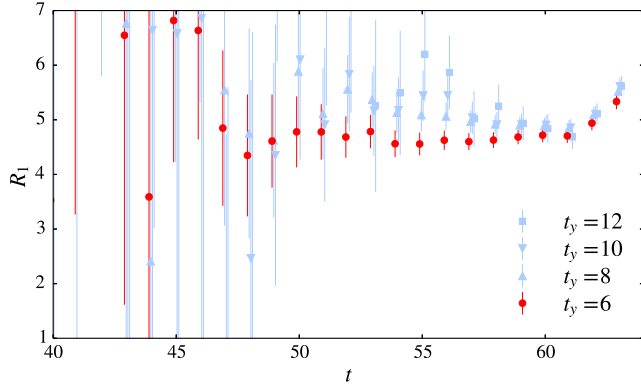| Ensemble	a/fm	Z_A
24^3	0.11	0.7019(26)
32^3	0.086	0.7396(17)

FIG. 5. The ratio $R_1(t, t_y)$ evaluated for different values of t_y on the 24^3, $m_l a = 0.005$ ensemble. $t_y = 6$ gives the cleanest signal and longest plateau. The points for different t_y have small horizontal offsets to help distinguish them on the plot.

IV. ANALYSIS

A. Correlator fits

We first calculate the three-point function on the 24^3 ensemble with $am_l = 0.005$ for values of t_y ranging from 6 to 18. Examining the data for R_1 (see Fig. 5), it is clear that

the best signal is achieved with $t_y = 6$. We therefore choose $t_y = 6$ for our analysis on the 24^3 ensembles and $t_y = 8$ on the 32^3 ensembles because it corresponds to the same physical distance.

Figure 6 shows the ratios R_1, R_2, R_3 and R_4 calculated on the 24^3, $m_l a = 0.005$ ensemble, and Fig. 7 shows the vector and pseudoscalar effective-mass plots. In all cases, we estimate the statistical error with a single-elimination jackknife. The two-point functions are fitted to a single exponential to extract Z_B and Z_{B^*}. Using these values of $Z_{B^{(*)}}$, we then fit the ratios to a constant in the regions given in Table IV where we expect excited-state contamination to be small. We choose the fit ranges for each ratio such that we obtain a good correlated χ^2/dof, and apply them to all ensembles of the same lattice spacing consistently.

From the ratios we use the procedure described in the previous section to extract g_b on each ensemble, giving the values listed in Table V.

B. Chiral and continuum extrapolations

We perform a chiral extrapolation using the SU(2) HMχPT formula for the axial coupling matrix element derived in [45]:
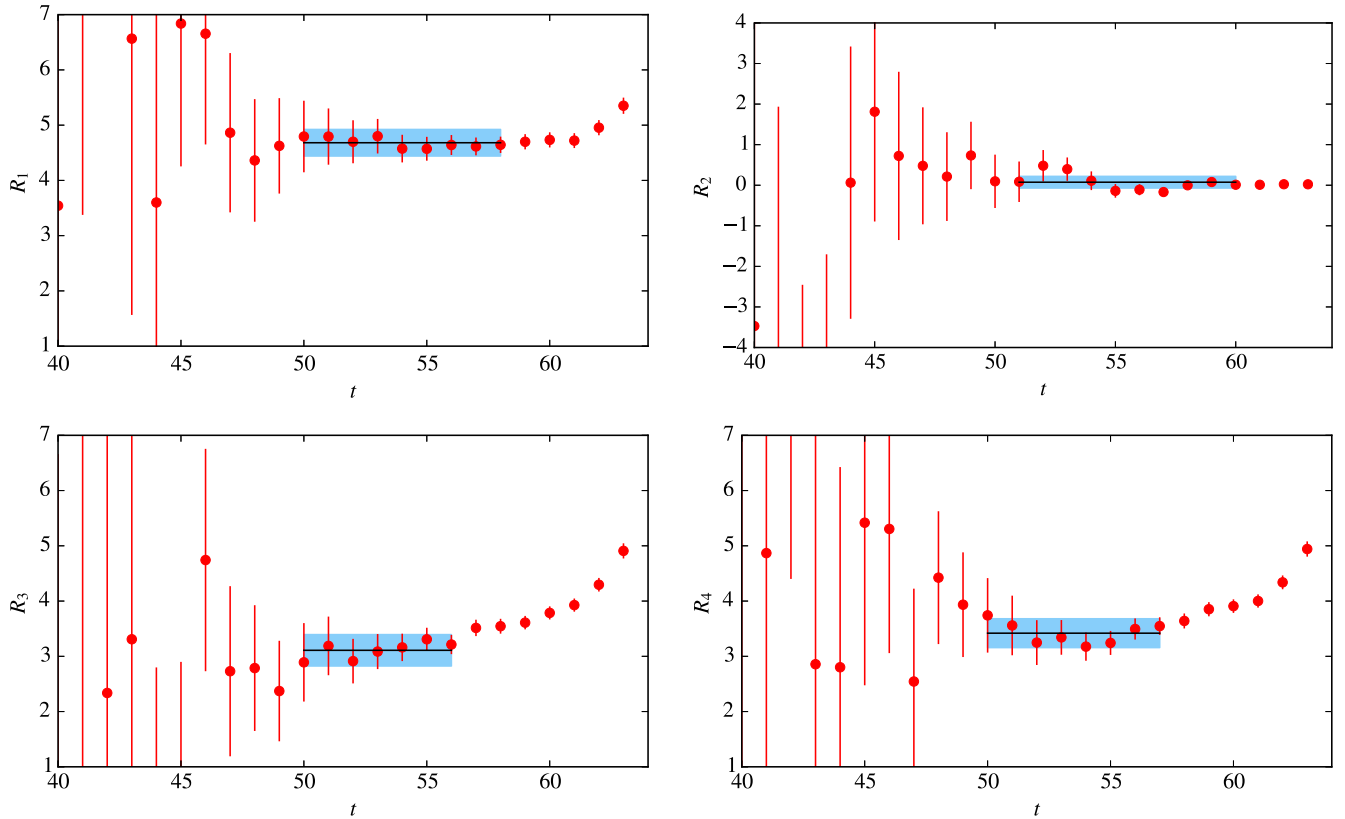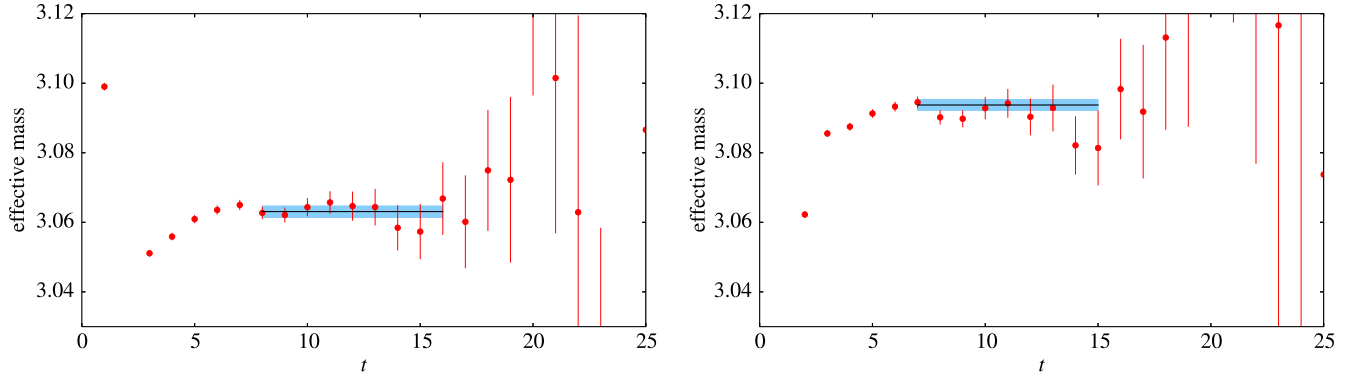

FIG. 6. Ratios $R_1(t, t_y)$, $R_2(t, t_y)$, $R_3(t, t_y)$ and $R_4(t, t_y)$ for $t_y = 6$ on the 24^3, $m_l a = 0.005$ ensemble. R_1 is calculated with $\vec{p} = \vec{p}' = 0$, the other ratios with $\vec{p} = (1, 0, 0)2\pi/L$, $\vec{p}' = 0$.

FIG. 7. B-meson (left) and B^*-meson (right) effective masses on the 24^3, $m_l a = 0.005$ ensemble.

$$g_b = g_0 \left(1 - \frac{2(1 + 2g_0^2)}{(4\pi f_\pi)^2} M_\pi^2 \log \frac{M_\pi^2}{\mu^2} + \alpha M_\pi^2 + \beta a^2 \right),$$

(28)

which is next-to-leading order in the chiral expansion, but only leading order in the heavy-quark expansion. We parametrize the light-quark and gluon discretization effects with an a^2 term, as expected for the domain-wall

TABLE IV.   Fit ranges used for the two-point functions and the ratios. For nonzero momenta, equivalent combinations are averaged. Fit ranges are the same for different light-quark masses at the same lattice spacing, *except* in the case of the B^* two-point function with momentum $(1, 1, 0)$ on 24^3, $m_l a = 0.020$ for which a range 7–15 is used in place of 9–15 listed in the table.

		Fit range $t_{\min} - t_{\max}$	
	$\vec{p}a/(2\pi/L)$	24^3	32^3
B	$(0, 0, 0)$	8–16	8–17
B^*	$(0, 0, 0)$	7–15	8–16
R_1	$(0, 0, 0)$	50–58	50–58
B^*	$(1, 0, 0)$	7–15	8–16
R_2	$(1, 0, 0)$	51–60	47–55
R_3	$(1, 0, 0)$	50–56	46–55
R_4	$(1, 0, 0)$	50–57	47–56
B^*	$(1, 1, 0)$	9–15	10–16
R_2	$(1, 1, 0)$	51–60	47–55
R_3	$(1, 1, 0)$	49–55	46–55
R_4	$(1, 1, 0)$	51–57	46–54

TABLE V.   Results for g_b on the 24^3 and 32^3 ensembles. Errors for g_b are statistical. Pion masses are from [26].

L/a	$m_l a$	M_π^2/GeV^2	g_b
24	0.005	0.108	0.533 ± 0.027
24	0.010	0.175	0.568 ± 0.023
24	0.020	0.311	0.580 ± 0.035
32	0.004	0.084	0.548 ± 0.020
32	0.006	0.119	0.603 ± 0.016
32	0.008	0.155	0.596 ± 0.018

light-quark and Iwasaki gauge actions. The lattice-spacing dependence from the RHQ action is more complicated. However, we argue in the next section that heavy-quark discretization effects are negligible and that an extrapolation in a^2 captures the leading scaling behavior. We use the PDG value [46] of the pion decay constant, $f_\pi = 130.4$ MeV.

Figure 8 shows the chiral-continuum extrapolation of the numerical simulation data to the physical light-quark mass and continuum using Eq. (28). The values of Z_A, as calculated in [25] and [26], are included for each ensemble. The statistical errors in Z_A are added in quadrature to the Monte-Carlo statistical errors in the lattice data for g_b before performing the chiral fit. The six ensembles are statistically independent, hence the fit is calculated by minimizing an uncorrelated χ^2 function. The parameters that minimize the χ^2 are $g_0 = 0.515$, $\alpha = -1.324$ GeV^{-2}, $\beta = -0.648$ GeV^2. We use these fitted parameters and their covariance matrix to estimate the error bands in our plots
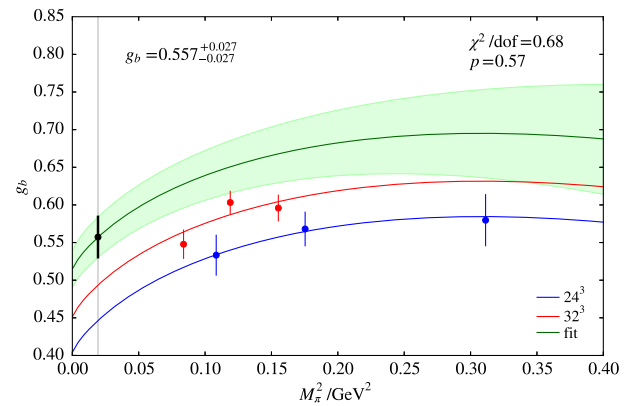

FIG. 8.   Chiral and continuum extrapolation. The bottom (blue) curve is the fit through the 24^3 ensemble points. The (red) curve above is the fit through the 32^3 ensemble points and the (green) error band and curve show the continuum extrapolation. The intersection with the vertical grey line corresponds to the physical pion mass. The result at the physical mass is shown by the (black) point with error.

and to give the errors in g_b. Our fitted result is $g_b = 0.557 \pm 0.027$.

V. SYSTEMATIC ERRORS

A. Chiral extrapolation

Our chiral extrapolation relies on NLO SU(2) HMχPT with pion masses above 400 MeV. Therefore we may be using the theory beyond its range of applicability and we are certainly omitting higher order terms in the chiral expansion. To estimate the uncertainty this introduces we consider a range of possible fits. First, we consider the effect of neglecting the heaviest mass from each ensemble (center left plot in Fig. 9). This alters the form of the fit dramatically but does not significantly change the final result. In the bottom row of Fig. 9 we replace f_π in the
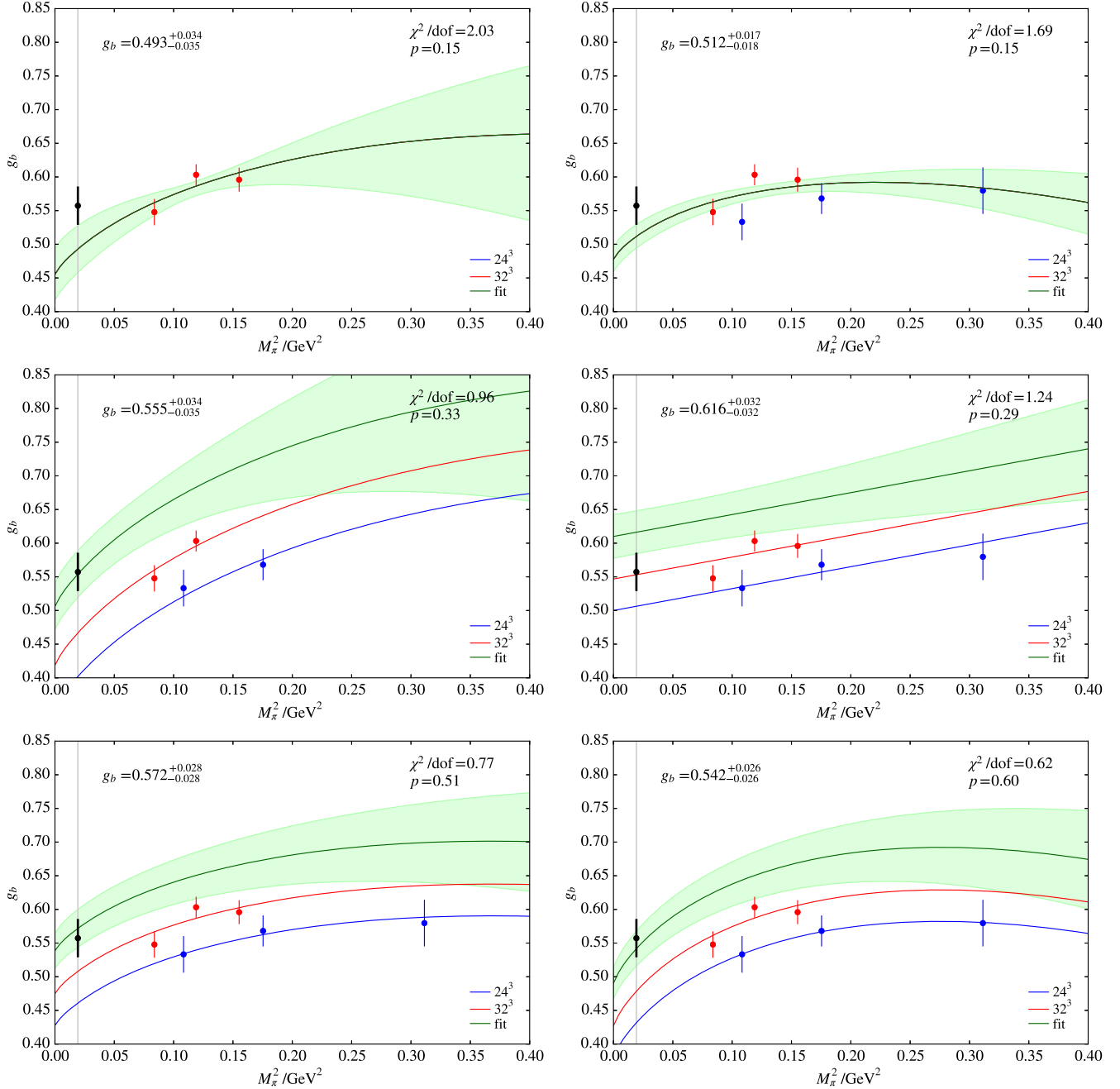

FIG. 9.   Variations of chiral fits. Top left: 32^2 data points only; top right: data points from both lattices with no a^2 term. Center left: heaviest masses dropped; center right: fit to a function linear in M_π^2. Bottom left: replacing f_π with $f_K = 156.1$ MeV; bottom right: replacing f_π with $f_0 = 112$ MeV. In each plot, the result of the preferred fit from Fig. 8 is shown as the black point, with error, on the vertical line at the physical pion mass.

coefficient of the NLO chiral logarithms with $f_K = 156.1$ MeV [46] or with $f_0 = 112$ MeV in the SU(2) chiral limit from the RBC/UKQCD light pseudoscalar meson analysis [26]. This changes the relative size of NLO and NNLO and higher-order terms in the chiral expansion. Finally, we note that our data does not show any strong evidence of chiral log curvature, presumably because our lightest data point corresponds to $M_\pi \approx 289$ MeV and is still rather heavy. We therefore consider an analytic fit, shown in the center right plot of Fig. 9, where we extrapolate linearly in M_π^2. Of these variations, the largest difference from our central value for g_b is from the linear fit in M_π^2 and a^2. This value is larger than our full chiral-continuum fit by 10.6%. Because the chiral and continuum extrapolations are treated together in our fitting procedure, however, discretization and chiral extrapolation errors cannot be fully disentangled. In Sec. V E 2 below we consider light-quark and gluon discretization errors, estimating a systematic error of 11.5%. This is the largest deviation seen in the chiral-continuum fits in Fig. 9 and is therefore the error we take for the combined chiral and continuum extrapolation.

B. Lattice-scale uncertainty

The coupling g_b is a dimensionless number calculated from ratios of correlators, so it should have only a mild dependence on the physical value of the lattice spacing. However, variations in a affect the chiral and continuum extrapolations. We estimate the error in g_b due to the lattice-spacing uncertainty by varying the 24^3 and 32^3 lattice spacings by their quoted (statistical plus systematic) uncertainties, σ_{24} and σ_{32} [26], one at a time whilst keeping the other fixed. Shifting the lattice spacing on the finest ensemble changes g_b by 0.7%, and on the coarser ensemble g_b changes by 0.6%. Therefore ascribing an error of 0.9% (the sum in quadrature) to this source of uncertainty seems a conservative estimate.

C. Unphysical sea strange-quark mass

Our simulation is performed with a sea strange-quark mass that differs from the physical value by approximately 10%. To investigate the effect of the sea strange-quark mass on g_b we use results from [45] for the NLO axial current matrix element in partially quenched HMχPT. This allows us to evaluate the expression with different valence and sea strange-quark masses. The NLO matrix element has four different contributions, coming from so-called sunset diagrams, wave-function renormalization, tadpole diagrams and the NLO analytic terms. We have calculated the effect of a 10% change in the sea strange-quark mass in the loop diagrams, assuming the values of the low-energy constants obtained from our preferred chiral fit, on the value of the coupling g_b. We find a change in g_b of 1.5%. This result is numerically consistent with the effect of the

strange sea-quark mass on the pion decay constant observed by the RBC/UKQCD collaboration in [26]. Therefore we ascribe an error of 1.5% in g_b due to the unphysical strange-quark mass.

D. RHQ parameter uncertainties

1. Statistical

To test the dependence of g_b on the uncertainties in the tuned RHQ parameters we calculate the coupling on the 24^3 $m_l a = 0.005$ ensemble using the full "box" of RHQ parameters used to interpolate to the tuned values:

$$\begin{bmatrix} m_0 a \\ c_p \\ \zeta \end{bmatrix}, \quad \begin{bmatrix} m_0 a \pm \sigma_{m_0 a} \\ c_p \\ \zeta \end{bmatrix}, \quad \begin{bmatrix} m_0 a \\ c_p \pm \sigma_{c_p} \\ \zeta \end{bmatrix}, \quad \begin{bmatrix} m_0 a \\ c_p \\ \zeta \pm \sigma_\zeta \end{bmatrix}. \tag{29}$$

For our 24^3 ensembles, the box parameters are given by

$$(m_0 a, c_p, \zeta) = (8.40, 5.80, 3.20),$$
$$(\sigma_{m_0 a}, \sigma_{c_p}, \sigma_\zeta) = (0.15, 0.45, 0.30). \tag{30}$$

We then linearly interpolate g_b to the point of the tuned parameters. By following this procedure underneath the jackknife we can propagate the statistical errors from parameter tuning through to g_b. Comparison of this determination to the result calculated directly using the tuned values of the parameters gives a measure of how sensitive g_b is to the uncertainties arising from the tuning. We find that the central values differ by 0.01% and the errors agree to two significant figures. In the context of the overall uncertainty this can be considered negligible.

Figure 10 shows g_b calculated on the seven sets of parameters indicated in Eq. (29) for the 24^3 $m_l a = 0.005$ ensemble.

2. Systematic

We also consider the effect on g_b of systematic uncertainties in the RHQ parameters. These are estimated in Ref. [31] and given in Table II. The three significant contributors are heavy-quark discretization effects, uncertainty in the lattice spacing, and uncertainty from the experimental inputs. To determine the sensitivity of g_b to these uncertainties we use the calculation on the box of parameters, Eq. (29), described in the previous subsection. We assume a linear dependence of g_b on the RHQ parameters for small shifts, then shift one parameter at a time by each systematic uncertainty and take the overall error as the effect of each of these shifts added in quadrature. The combined effect, shown in Table VI, is an error of 1.5% in g_b.
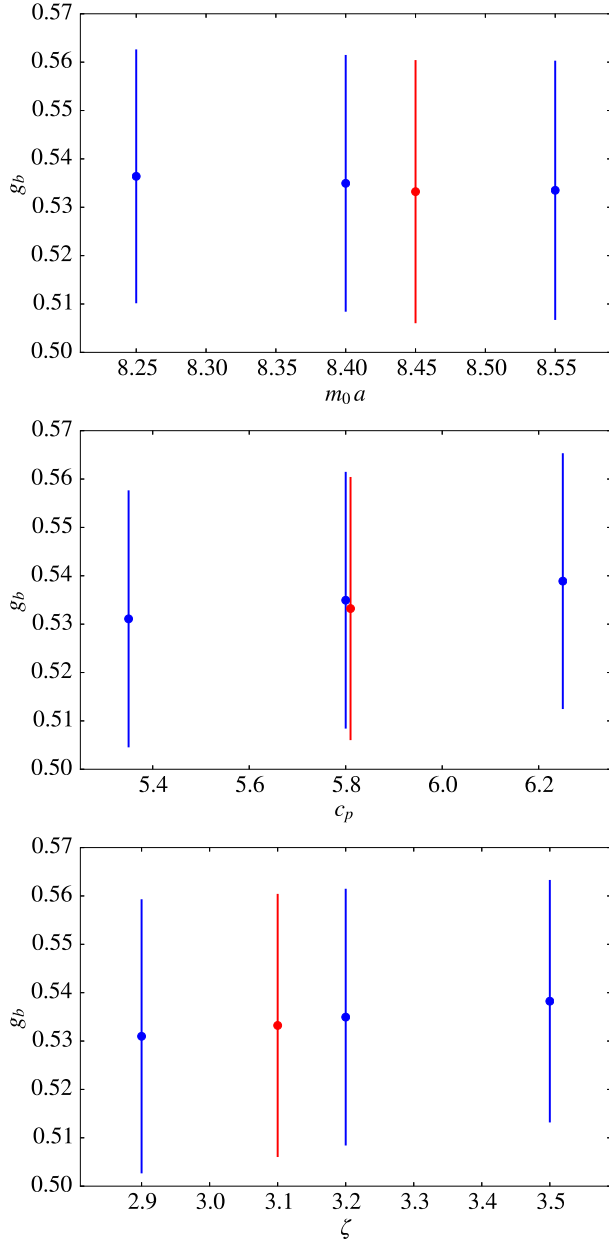
FIG. 10. g_b calculated for the sets of RHQ parameters used to define the parameter "box" on the 24^3 $m_l a = 0.005$ ensemble. The blue points are the results for the box parameter choices and the red point shows g_b calculated directly at the tuned parameter values.

TABLE VI. The effect of systematic uncertainties in the RHQ parameters on g_b. Each parameter was shifted by the uncertainty from each source and the effect on g_b calculated by assuming g_b depends linearly on the parameters.

| Source | % error from parameter | | | |
	$m_0 a$	c_p	ζ	Total
HQ discretization	0.25	0.65	0.30	0.76
Lattice scale	0.97	0.65	0.24	1.19
Experimental inputs	0.14	0.33	0	0.35
Total	1.01	0.98	0.38	1.46

effective theories. Oktay and Kronfeld [48] have catalogued the relevant operators and calculated the mismatch coefficients at tree level.

Because we are evaluating a matrix element of the light-quark axial-vector current, heavy-quark discretization errors stem from mismatches in higher-dimension operators in the heavy-quark action which correct the B and B^* meson masses. We expect these effects to be negligible. From our tuning procedure [31] we can relate changes in the meson masses to changes in the RHQ parameters $m_0 a$, c_p and ζ, while in Sec. V D below, we relate changes in the RHQ parameters to changes in g_b. Hence we can estimate the effect of errors in the meson masses on g_b.

In Appendix C of [31], we estimated the heavy-quark discretization error on the spin-averaged B_s meson mass as 0.05%. Also in [31], that spin-averaged mass was most sensitive to variations in $m_0 a$, with a 0.05% shift corresponding to a change of around 0.02 in $m_0 a$ on the 24^3 $m_l a = 0.005$ ensemble. From Sec. V D, shifting $m_0 a$ by the half-width of our tuning box changes g_b by no more than 1.5%. For the 24^3 $m_l a = 0.005$ ensemble, this shift in $m_0 a$ is 0.15 and hence we expect a heavy-quark discretization error on g_b of no more than $(0.02/0.15) \times 1.5\% = 0.2\%$, which is negligible compared to our overall uncertainty.

2. Light-quark and gluon discretization errors

Leading discretization errors from the domain-wall light-quark action and the Iwasaki gauge action are both $O(a^2)$ and are included as an a^2 term in the combined chiral-continuum extrapolation. However the data is also compatible within errors with assuming no lattice-spacing dependence; a fit with no a^2 term also yields an acceptable, albeit larger, χ^2/dof. The top row of Fig. 9 shows chiral fits to the data without an a^2 term. To estimate the systematic errors coming from the continuum extrapolation we use the difference of 11.5% in g_b between a fit to our finest data set ($a \approx 0.086$ fm) and the a^2 extrapolation using both lattice spacings. This is the largest effect in all variations of our chiral and continuum extrapolations and is therefore the value appearing in Table VII for the combined chiral and continuum extrapolation uncertainty.

E. Discretization errors

1. Heavy-quark discretization errors

We estimate heavy-quark discretization errors using an effective field theory approach [39,47,48] in which both our lattice theory and QCD are described by effective continuum Lagrangians built from the same operators and errors stem from mismatches between the short-distance coefficients of higher-dimension operators in the two

TABLE VII. Error budget for systematic and statistical errors.

Statistical errors	4.8%
Chiral and continuum extrapolation	11.5%
Lattice scale uncertainty	0.9%
Finite volume effects	1.0%
RHQ parameter uncertainties	1.5%
Unphysical sea strange-quark mass	1.5%
Systematic errors total	11.8%

F. Finite-volume effects

We expect that finite-volume effects are small since there are no propagating light particles in the simulated system. To estimate their size we compare the value of g_b obtained from an NLO heavy-meson χPT fit to our data, with and without finite volume effects included. We compare the finite and infinite-volume fit result at all of our simulated pion-mass values. The largest finite-volume correction, which occurs for our lightest pion mass, is $\lesssim 1\%$, so we take 1% as the finite-volume error in our calculation of g_b.

VI. CONCLUSIONS

The sum in quadrature of all the systematic errors described in Sec. V gives a total systematic uncertainty of 12%. Our final error budget is given in Table VII and our final value of the coupling g_b including statistical and systematic errors is

$$g_b = 0.56(3)_{\text{stat}}(7)_{\text{sys}}. \tag{31}$$

Our calculation is the first directly at the physical b-quark mass, and has a complete systematic error budget. Figure 11 compares our result to earlier dynamical calculations at the charm-quark mass and in the static limit. The dependence of g on the value of the heavy-quark mass is mild, and our result lies in the region that would be expected from interpolating between the charm- and infinite-mass determinations. Our result is compatible with the experimental value $g_c^{\text{exp}} = 0.570 \pm 0.004 \pm 0.005$ extracted from the natural linewidth of the transition
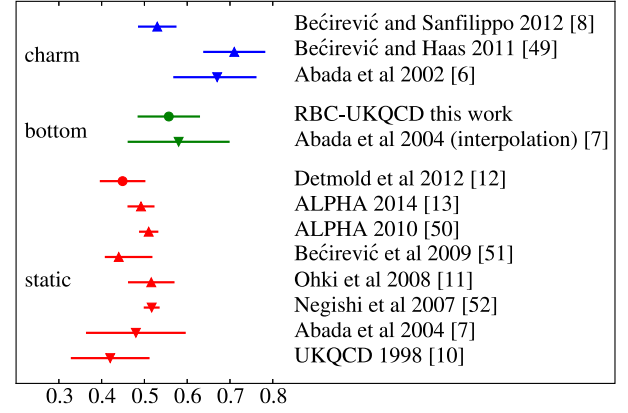

FIG. 11. Comparison of quenched (downward triangles), $N_f = 2$ (upward triangles) and $N_f = 2 + 1$ (circles) calculations of the couplings g_c, g_b and $\hat{g}$ [6–8,10–13,49–52]. Error bars represent the sum in quadrature of all quoted errors (statistical and systematic).

$D^*(2010)^+ \to D^0\pi^+$ by the *BABAR* collaboration in [17]. This further suggests that $1/m_Q^n$ corrections to the coupling g are small. Our result has been used by the RBC/UKQCD collaboration in the chiral extrapolations of numerical lattice data for the B-meson leptonic decay constants [32,33] and $B \to \pi\ell\nu$ and $B_s \to K\ell\nu$ semileptonic form factors [34,35].

ACKNOWLEDGMENTS

[1] J. Charles, A. Höcker, H. Lacker, S. Laplace, F. R. Le Diberder, J. Malclés, J. Ocariz, M. Pivk, and L. Roos, Eur. Phys. J. C **41**, 1 (2005).

[2] M. Bona *et al.*, J. High Energy Phys. 05 (2005) 028.

[3] J. Laiho, E. Lunghi, and R. S. Van de Water, Phys. Rev. D **81**, 034503 (2010).

[4] J. Goity, Phys. Rev. D **46**, 3929 (1992).

[5] S. R. Sharpe and Y. Zhang, Phys. Rev. D **53**, 5125 (1996).

[6] A. Abada, D. Bećirević, Ph. Boucaud, G. Herdoiza, J. P. Leroy, O. Pène, and J. Rodríguez-Quintero, Phys. Rev. D **66**, 074504 (2002).

[7] A. Abada *et al.*, J. High Energy Phys. 04 (2004) 016.

[8] D. Bećirević and F. Sanfilippo, Phys. Lett. B **721**, 94 (2013).

[9] K. U. Can, G. Erkol, M. Oka, A. Ozpineci, and T. T. Takahashi, Phys. Lett. B **719**, 103 (2013).

[10] G. M. de Divitiis *et al.*, J. High Energy Phys. 98 (1998) 010.

[11] H. Ohki, H. Matsufuru, and T. Onogi, Phys. Rev. D **77**, 094509 (2008).

[12] W. Detmold, C.-J. Lin, and S. Meinel, Phys. Rev. D **85**, 114508 (2012).

[13] F. Bernardoni, J. Bulava, M. Donnellan, and R. Sommer (ALPHA Collaboration), Phys. Lett. B **740**, 278 (2015).

[14] S. Ahmed *et al.* (CLEO Collaboration), Phys. Rev. Lett. **87**, 251801 (2001).

[15] A. Anastassov *et al.* (CLEO Collaboration), Phys. Rev. D **65**, 032003 (2002).

[16] J. P. Lees *et al.* (*BABAR* Collaboration), Phys. Rev. Lett. **111**, 111801 (2013); **111**, 169902(E) (2013).

[17] J. P. Lees *et al.* (*BABAR* Collaboration), Phys. Rev. D **88**, 052003 (2013); **88**, 079902(E) (2013).

[18] P. Colangelo, G. Nardulli, A. Deandrea, N. Di Bartolomeo, R. Gatto, and F. Feruglio, Phys. Lett. B **339**, 151 (1994).

[19] V. Belyaev, V. Braun, A. Khodjamirian, and R. Rückl, Phys. Rev. D **51**, 6177 (1995).

[20] H. Dosch and S. Narison, Phys. Lett. B **368**, 163 (1996).

[21] P. Colangelo and F. De Fazio, Eur. Phys. J. C **4**, 503 (1998).

[22] T.-M. Yan, H.-Y. Cheng, C.-Y. Cheung, G.-L. Lin, Y. C. Lin, and H.-L. Yu, Phys. Rev. D **46**, 1148 (1992).

[23] M. Wise, Phys. Rev. D **45**, R2188 (1992).

[24] R. Casalbuoni, A. Deandrea, N. Di Bartolomeo, R. Gatto, F. Feruglio, and G. Nardulli, Phys. Rep. **281**, 145 (1997).

[25] C. Allton *et al.* (RBC-UKQCD Collaboration), Phys. Rev. D **78**, 114509 (2008).

[26] Y. Aoki *et al.*, Phys. Rev. D **83**, 074508 (2011).

[27] Y. Iwasaki, arXiv:1111.7054.

[28] Y. Iwasaki and T. Yoshié, Phys. Lett. B **143**, 449 (1984).

[29] D. B. Kaplan, Phys. Lett. B **288**, 342 (1992).

[30] Y. Shamir, Nucl. Phys. **B406**, 90 (1993).

[31] Y. Aoki, N. H. Christ, J. M. Flynn, T. Izubuchi, C. Lehner, M. Li, H. Peng, A. Soni, R. S. Van de Water, and O. Witzel (RBC and UKQCD Collaborations), Phys. Rev. D **86**, 116003 (2012).

[32] O. Witzel, *Proc. Sci.*, LATTICE2012 (2012) 103 [arXiv:1211.3180].

[33] N. H. Christ, J. M. Flynn, T. Izubuchi, T. Kawanai, C. Lehner, A. Soni, R. S. Van de Water, and O. Witzel (RBC and UKQCD Collaborations), Phys. Rev. D **91**, 054502 (2015).

[34] T. Kawanai, R. S. Van de Water, and O. Witzel, *Proc. Sci.*, LATTICE2012 (2012) 109 [arXiv:1211.0956].

[35] J. M. Flynn, T. Izubuchi, T. Kawanai, C. Lehner, A. Soni, R. S. Van de Water, and O. Witzel (RBC and UKQCD Collaborations), Phys. Rev. D **91**, 074510 (2015).

[36] E. Eichten and B. Hill, Phys. Lett. B **234**, 511 (1990).

[37] W. Detmold, C.-J. D. Lin, and S. Meinel, Phys. Rev. Lett. **108**, 172003 (2012).

[38] G. Lepage, Nucl. Phys. B, Proc. Suppl. **26**, 45 (1992).

[39] A. X. El-Khadra, A. S. Kronfeld, and P. B. Mackenzie, Phys. Rev. D **55**, 3933 (1997).

[40] S. Aoki, Y. Kuramashi, and S.-i. Tominaga, Prog. Theor. Phys. **109**, 383 (2003).

[41] N. Christ, M. Li, and H.-W. Lin, Phys. Rev. D **76**, 074505 (2007).

[42] B. Sheikholeslami and R. Wohlert, Nucl. Phys. **B259**, 572 (1985).

[43] H.-W. Lin and N. Christ, Phys. Rev. D **76**, 074506 (2007).

[44] R. G. Edwards and B. Joo, Nucl. Phys. B, Proc. Suppl. **140**, 832 (2005).

[45] W. Detmold, C.-J. Lin, and S. Meinel, Phys. Rev. D **84**, 094502 (2011).

[46] J. Beringer *et al.*, Phys. Rev. D **86**, 010001 (2012).

[47] K. Symanzik, Nucl. Phys. **B226**, 187 (1983).

[48] M. B. Oktay and A. S. Kronfeld, Phys. Rev. D **78**, 014504 (2008).

[49] D. Bećirević and B. Haas, Eur. Phys. J. C **71**, 1734 (2011).

[50] J. Bulava, M. A. Donnellan, and R. Sommer, *Proc. Sci.*, LATTICE2010 (2010) 303 [arXiv:1011.4393].

[51] D. Bećirević, B. Blossier, E. Chang, and B. Haas, Phys. Lett. B **679**, 231 (2009).

[52] S. Negishi, H. Matsufuru, and T. Onogi, Prog. Theor. Phys. **117**, 275 (2007).